Inorganic Chemistry

Article

pubs.acs.org/IC

Synthesis and Structural/Physical Properties of $U_3Fe_2Ge_7$: A Single-Crystal Study

Margarida S. Henriques,[*,†,‡] Denis I. Gorbunov,[*,†,§] João C. Waerenborgh,[‡] Mathieu Pasturel,[∥] Alexander V. Andreev,[†] Michal Dušek,[†] Yurii Skourski,[§] Ladislav Havela,[⊥] and António P. Gonçalves[‡]

[†]Institute of Physics, Academy of Sciences of the Czech Republic, Na Slovance 2, 182 21 Prague, Czech Republic

[‡]Centro de Ciências e Tecnologias Nucleares, Instituto Superior Técnico, Universidade de Lisboa, P-2695-066 Bobadela, Portugal

[§]Dresden High Magnetic Field Laboratory (HLD-EMFL), Helmholtz-Zentrum Dresden-Rossendorf, D-01314 Dresden, Germany

[∥]Institut des Sciences Chimiques de Rennes, Chimie du Solide et Matériaux, Université Rennes 1, UMR CNRS 6226, 263 Avenue du Général Leclerc, 35042 Rennes, France

[⊥]Department of Condensed Matter Physics, Faculty of Mathematics and Physics, Charles University, Ke Karlovu 5, 121 16 Prague, Czech Republic

Supporting Information

ABSTRACT: A single crystal of $U_3Fe_2Ge_7$ was synthesized by the tin-flux method, and its structural and electronic properties were studied. The compound crystallizes in the orthorhombic crystal structure of $La_3Co_2Sn_7$ type with two Wyckoff sites for the U atoms. $U_3Fe_2Ge_7$ displays a ferromagnetic order below T_C = 62 K. Magnetization measurements in static (up to 14 T) and pulsed (up to 60 T) magnetic fields revealed a strong two-ion uniaxial magnetic anisotropy. The easy magnetization direction is along the *c* axis and the spontaneous magnetic moment is 3.3 μ_B per formula unit at 2 K. The moment per Fe atom is 0.2 μ_B, as follows from Mössbauer spectroscopy. The magnetic moments are oriented perpendicular to the shortest inter-uranium distances that occur within the zigzag chains in the *ab* plane, contrary to other U-based isostructural compounds. The magnetization along the *a* axis reveals a first-order magnetization process that allows for a quantitative description of the magnetic anisotropy in spite of its enormous energetic strength. The strong anisotropy is reflected in the specific heat and electrical resistivity that are affected by a gap in magnon spectrum.

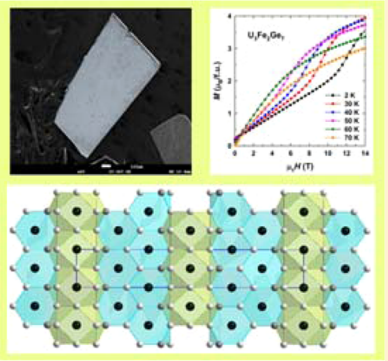

1. INTRODUCTION

Uranium intermetallic compounds display a rich variety of magnetic properties depending on the character of the 5f electronic states. They are mainly determined by the hybridization of the 5f states with outer states of ligand atoms. For example, the properties of U−Fe intermetallics critically depend on the 5f−3d hybridization. No ordered magnetic moments are formed in UFeAl, although both the U and Fe sublattices could in principle be magnetic.[1] Contrary to that, in UFe_2, both sublattices are magnetic, although magnetic moments are undoubtedly strongly affected by the hybridization.[2−4] It is therefore very interesting to study variations of the 5f and 3d magnetism in numerous ternaries, including both U and Fe with different stoichiometry and diverse coordinations.

The important role of the mutual hybridization of the 5f and 3d states as well as the hybridization with other types of states follows from the magnetic properties of compounds existing in the U−Fe−Ge phase diagram, documented for the isothermal section at 900 °C.[5] In $U_9Fe_7Ge_{24}$ (tetragonal structure), a sizable U-5f and Ge-4p overlap exists.[6] The 3d Fe states are also substantially delocalized, and a paramagnetic behavior was observed down to 2 K. U_2Fe_3Ge (hexagonal structure) and $U_3Fe_4Ge_4$ (orthorhombic structure) are itinerant ferromagnets.[7−12] Their magnetism is dominated by the uranium; no intrinsic Fe magnetic moment is formed. While $U_3Fe_4Ge_4$ exhibits a strong uniaxial magnetic anisotropy with the anisotropy field μ_0H_a exceeding 60 T, U_2Fe_3Ge is much less anisotropic (μ_0H_a = 8 T), not typical of uranium intermetallic compounds. Furthermore, $U_{33}Fe_{3.32}Ge_{34}$ (tetragonal structure) orders ferromagnetically below 28 K and has a pronounced magnetic hysteresis ruled by the U sublattice and its anisotropy.[13]

Besides the compounds mentioned, a further representative of the U−Fe−Ge phase diagram is known.[5] It is $U_3Fe_2Ge_7$, a compound with an orthorhombic crystal structure of the $La_3Co_2Sn_7$ type.[14]

Some uranium intermetallic compounds with the 3−2−7 stoichiometry have already been characterized. $U_3Co_2Ge_7$ was reported to be an itinerant ferromagnet below about 40 K.[15−17] However, in ref 16, a possibility of ferrimagnetic or noncollinear ferromagnetic structure was also considered. Strong uniaxial magnetic anisotropy was found with the *b* axis (the longest one) being the easy-magnetization direction.[15,16] The

Received: August 3, 2015
Published: September 15, 2015

DOI: 10.1021/acs.inorgchem.5b01736
Inorg. Chem. 2015, 54, 9646−9655

magnetism is expected to originate predominantly from the U sublattice, as the Co and Ge magnetic moments were calculated to be lower than 0.1 μ_B. The Sommerfeld coefficient for $U_3Co_2Ge_7$ is γ = 65−87 mJ mol_U^{-1} K^{-1}. Furthermore, two compounds with Si instead of Ge are known.[18−21] $U_3Ru_2Si_7$ is an itinerant system that displays a magnetic order below 29 K, whereas $U_3Fe_2Si_7$ exhibits no magnetic order down to 4.2 K.

In the present work we report the synthesis of single crystals of the novel intermetallic compound $U_3Fe_2Ge_7$ by the flux method and its structural and electronic properties. The single-crystal studies have revealed that $U_3Fe_2Ge_7$ crystallizes with a structure of the orthorhombic isotype $La_3Co_2Sn_7$. The main structural feature of $U_3Fe_2Ge_7$ is larger interatomic distances between U, Fe, and their ligand atoms when compared to the compounds of the system U−Fe−Ge mentioned above. The hybridization is therefore expected to be reduced, leading to distinct magnetic and other electronic properties. The compound orders ferromagnetically at 62 K and displays large magnetocrystalline anisotropy. The influence of high magnetic fields on magnetization in all principal directions has been determined. The temperature dependence of the specific heat and resistivity reveals the influence of magnons with an anisotropy gap.

2. EXPERIMENTAL SECTION

Single crystals of $U_3Fe_2Ge_7$ were prepared by the molten-metal flux method starting from a 1:1:1 ratio of the elements U, Fe, and Ge (with purities of 99.95% for U and 99.999% for Fe and Ge) loaded in a graphite crucible, together with a 10 times larger molar amount of Sn (99.999% pure) used as a flux. The crucible was then inserted into an evacuated silica tube, filled with Ar, flame-sealed, and held in an oven at 1273 K for 2 days, followed by cooling to 573 K at the rate of 5 K/h. At this temperature the liquid Sn was removed by centrifugation and the samples were cooled to room temperature. The crystals were then cleaned by a diluted solution of hydrochloric acid (10%). The plate-like crystals shown in Figure 1 were observed by scanning electron

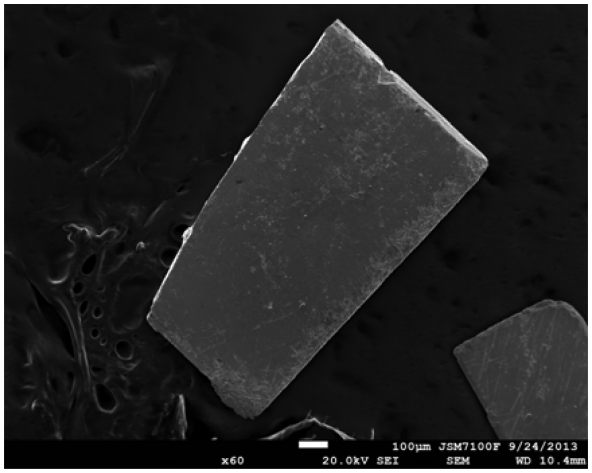

Figure 1. Secondary electron SEM image of $U_3Fe_2Ge_7$ single crystals grown by the Sn-flux method. The crystals were taken from the crucible and cleaned with a diluted solution of hydrochloric acid.

microscopy (SEM), and their chemical composition was found to be 25U:17Fe:58Ge, as given by energy-dispersive X-ray spectroscopy (EDS) in a JEOL-JSM 6400 apparatus. The measurements were carried out with the electron beam operating at 15 kV, and at least three points on the crystal surface were analyzed. Despite the use of Sn as flux, no traces of this element were found within the spectrometer detection limit. According to refs 14, 16, 17, and 22, the sample preparation from the starting stoichiometries $U_3Co_2Ge_7$, $U_3Co_4Ge_7$, and $U_2Co_3Ge_5$ yields similar results using a 20-fold quantity of Sn.

Single-crystal X-ray diffraction was undertaken in order to determine details of the crystal structure of $U_3Fe_2Ge_7$, since (i) the formation of $U_3Co_2Ge_7$ with a tetragonal crystal structure was not excluded in ref 16 and (ii) $U_3Ru_2Si_7$ was reported to have a disordered Ru−Si sublattice.[21] A small single crystal of dimensions 0.17 × 0.12 × 0.07 mm^3 suitable for X-ray diffraction was glued on the top of a glass fiber and mounted onto a goniometer head. The diffracted intensities were collected at ambient temperature using a Gemini four-circle diffractometer (Agilent), equipped with a Mo X-ray tube (λ(Mo Kα) = 0.71073 Å), Mo-Enhance collimator, graphite monochromator, and Atlas CCD detector. The CrysAlis[23] software was used to collect and process the data, and the program X-Shape[24] was employed for face indexing of the crystal shape, necessary to perform the accurate absorption correction in combination with a Gaussian correction based on spherical harmonic functions. The Superflip[25] program was used for structure solution, and Jana2006 package[26] for structure refinement based on F^2. Details on the data collection and refinement procedure, lattice parameters, and final refinement factors are given in Table 1.

Table 1. Details on the Single-Crystal Data Collection and Crystal Structure Refinement of $U_3Fe_2Ge_7$

chemical formula	$U_3Fe_2Ge_7$
formula weight(g mol^{-1})	1334
crystal system	orthorhombic
space group	*Cmmm* (No. 65)
lattice parameters (Å)	a = 4.1666(4)
	b = 24.982(2)
	c = 4.1557(3)
cell volume (Å^3)	432.57(6)
formula per unit cell (Z), calculated density (g cm^{-3})	2, 10.24
absorption coefficient (mm^{-1})	83
radiation, wavelength (Å)	Mo Kα, 0.710 73
θ range (deg)	3.3−29
data set	$-5 \le h \le 5$, $-31 \le k \le 31$, $-5 \le l \le 5$
collected/unique reflections/ R_{int}	3811/2083/0.202
refined parameters	14
final agreement factors ($I > 3\sigma(I)$) R, wR[a]	0.038, 0.110
goodness of the fit	1.79
extinction coefficient (×10^{-3})	5
highest/lowest peak of electron density (e$^-$ Å^{-3})	3.99/−3.33

[a] $R(F) = \sum||F_o| - |F_c||/|F_c|$, $wR_2 = \{\sum[w|F_o|^2 - |F_c|^2)^2]/\sum[w|F_o|^4]\}^{1/4}$, $w^{-1} = [\sigma^2(F_o)^2) + 7.27P]$, $P = \{\max[(F_o)^2,0] + 2(F_c)^2\}/3$.

The atomic coordinates and equivalent isotropic displacement parameters, as well as important interatomic distances, are listed in Table 2 and Table 3, respectively. Further details on the crystal structure investigation, including the CIF file, can be obtained from the Supporting Information.

Several crystals from the batch were crushed and ground into a powder for an X-ray diffraction experiment, which was carried out on a Panalytical X'Pert diffractometer (Bragg−Brentano θ−2θ geometry, Cu X-ray tube (λ(Cu Kα) = 1.54056 Å)). The intensity data were collected with 2θ from 10° to 90° with an exposure time of 5 s/step. The collected patterns matched very well the patterns simulated from the single-crystal X-ray diffraction data.

To perform measurements of the physical properties of the single crystals, their proper crystallographic orientation was needed. The first attempt was naturally made on one of the plate crystals using a conventional powder X-ray diffraction machine (Bragg−Brentano θ−2θ geometry). As shown in the experimental pattern in Figure 2, the

DOI: 10.1021/acs.inorgchem.5b01736
Inorg. Chem. 2015, 54, 9646−9655

Table 2. Atomic Coordinates and Equivalent Isotropic Displacement Parameters for $U_3Fe_2Ge_7$

atom	site	x	y	z	U_{eq} (Å^2)[b]
U1	2*a*	0	0	0	0.0059(4)
U2	4*j*	0	0.31640(4)	0.5	0.0074(4)
Fe1	4*i*	0	0.12817(16)	0.5	0.0105(8)
Ge1	2*c*	0.5	0	0.5	0.0092(8)
Ge2	4*i*	0	0.22070(11)	0	0.0087(6)
Ge3	4*i*	0	0.41286(12)	0	0.0112(7)
Ge4	4*j*	0	0.08727(12)	0.5	0.0100(6)

[b] U_{eq} is defined as one-third of the trace of the orthogonalized U_{ij} tensor.

Table 3. Selected Bond Lengths (Å) for $U_3Fe_2Ge_7$

atom pair		distance	atom pair		distance
U1	2Fe1	3.202(4)	Ge2	2U2	3.168(2)
	4Ge1	2.942(4)		4U2	3.085(1)
	4Ge3	3.013(2)		2Ge2	2.546(2)
	4Ge4	3.012(2)		1Fe1	2.312(5)
U2	4Fe1	3.252(1)	Ge3	2U1	3.013(2)
	2Ge4	3.183(2)		2U2	3.182(2)
	2Ge3	3.182(2)		2Ge1	3.009(2)
	4Ge2	3.085(1)		4Ge4	2.942(4)
	2Ge2	3.168(2)	Ge4	2Fe1	2.315(2)
Fe1	2Ge4	2.315(2)		2U1	3.012(2)
	2Ge3	2.322(2)		2U2	3.183(2)
	1Ge2	2.312(5)		2Ge1	3.016(2)
Ge1	4U1	2.942(4)		4Ge3	2.942(4)
	4Ge4	3.016(2)		2Fe1	2.315(2)
	4Ge3	3.009(2)			

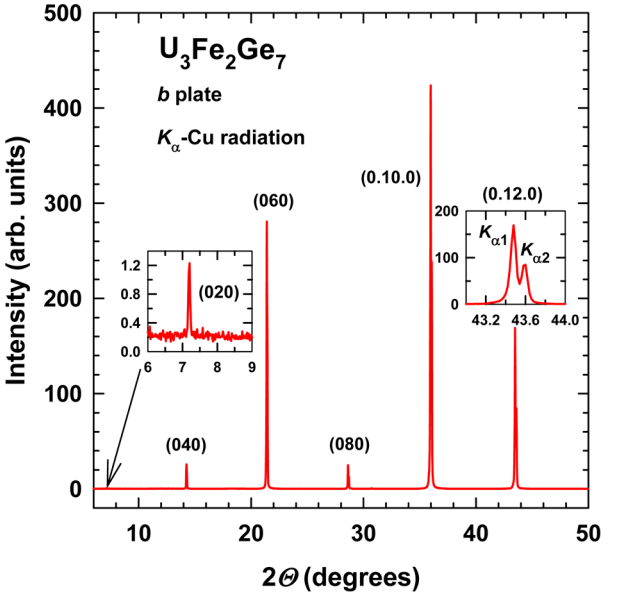

Figure 2. X-ray diffraction pattern obtained on a $U_3Fe_2Ge_7$ single crystal, showing that the crystal plate is oriented perpendicular to the crystallographic *b* axis seen even for very weak reflections (left inset). The reflections are narrow enough to distinguish the splitting of the $K_{\alpha1}-K_{\alpha2}$ doublet from the Cu radiation at $2\theta = 43°$ (right inset).

crystal plate was found to be perpendicular to the *b* axis. Nevertheless, due to the small dimensions of the grown crystals, the directions [100] and [001] of the orthorhombic lattice could be distinguished neither by this method nor by backscattered Laue diffraction.

As follows from the symmetry of the space group *Cmmm* adopted by $U_3Fe_2Ge_7$, the projection of the reciprocal lattice along the [001] direction reveals systematic absences that allow the distinction between [100] and [001], as given by the general reflection conditions for centered crystalline cells.[27] Thus, to find the proper orientation of the lattice of the $U_3Fe_2Ge_7$ single crystals, a single crystal of 2.1 × 1.5 × 0.3 mm^3 dimensions suitable for measurements of physical properties was tested in the above-mentioned four-circle diffractometer. A small set of reflections was measured with the primary beam focused on one of the crystal corners. These data were then indexed to find the crystal lattice, space group, cell parameters, and the expected centering along the *c* axis, as shown in Figure 3. Finally, by crystal

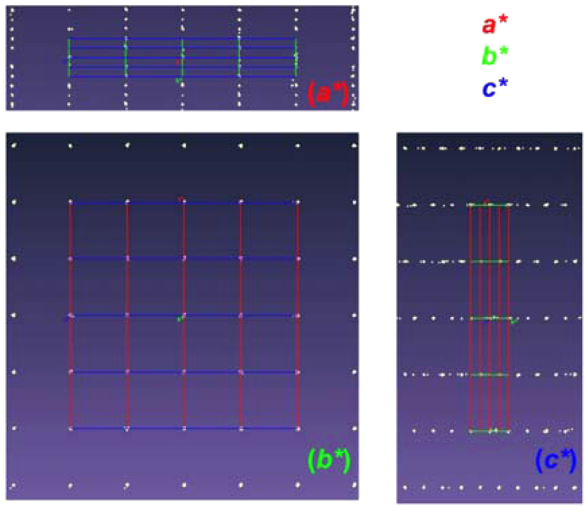

Figure 3. Experimental reconstruction of the reciprocal lattice of a $U_3Fe_2Ge_7$ single crystal. The centering along *c* as given by the general reflection conditions for the *Cmmm* space group is seen in the reciprocal lattice projection along *c**.

shape indexing the correspondence between the orthorhombic reciprocal lattice directions and the real crystal directions was found, allowing the distinction of the three crystallographic directions. Previous studies of other U-based isostructural intermetallic compounds (see Introduction) were performed without the distinction among the three crystallographic directions.

Temperature and field dependences of the magnetization between 2 and 300 K were measured along the principal crystallographic directions on the same 10 mg sample using a standard PPMS-14 magnetometer (Quantum Design) in magnetic fields up to 14 T. Magnetization curves in pulsed magnetic fields (pulse duration 20 ms) were measured by the induction method using a coaxial pick-up coil system.

PPMS-14 was also used for measurements of specific heat and electrical resistivity as functions of temperature. Specific heat was measured by the relaxation method; the electrical resistivity, by the four-contact technique with the excitation current $I = 1$ mA flowing in the *ac* plane.

^{57}Fe Mössbauer spectra were collected between 295 and 4 K in transmission mode using a conventional constant-acceleration spectrometer and a 25 mCi ^{57}Co source in a Rh matrix. The velocity scale was calibrated using α-Fe foil. Isomer shifts, IS, are given relative to this standard at room temperature. The absorbers were obtained by packing the powdered sample into a Perspex holder. Low-temperature spectra were collected in a bath cryostat with the sample immersed in liquid He for the measurement at 4.1 K and in He exchange gas for temperatures greater than 4.1 K. The spectra were fitted to Lorentzian lines using a nonlinear least-squares method.[28]

DOI: 10.1021/acs.inorgchem.5b01736
Inorg. Chem. 2015, 54, 9646−9655

3. RESULTS AND DISCUSSION

3.1. Crystal Chemistry. The structure refinement has confirmed that $U_3Fe_2Ge_7$ crystallizes in the orthorhombic isotype $La_3Co_2Sn_7$ (space group *Cmmm*). The lattice parameters for $U_3Fe_2Ge_7$ from the single-crystal data refinement are a = 4.167(7) Å, b = 24.982(2) Å, and c = 4.156(3) Å. The asymmetric unit for $U_3Fe_2Ge_7$ consists of seven different atomic sites, two for U, one for Fe, and four for Ge (Table 2). The refinement of site occupancies did not indicate any deviation from the full occupation or substitution in any of the atomic positions. This is in line with the fact that most of the known uranium compounds crystallizing in the $La_3Co_2Ge_7$ structure archetype are crystallographically ordered, except $U_3Ru_2Si_7$, which has disorder within the Ru−Si sublattice.[21]

Figure 4a displays the $U_3Fe_2Ge_7$ unit cell. This type of structure can be seen as an intergrowth of two fragments of

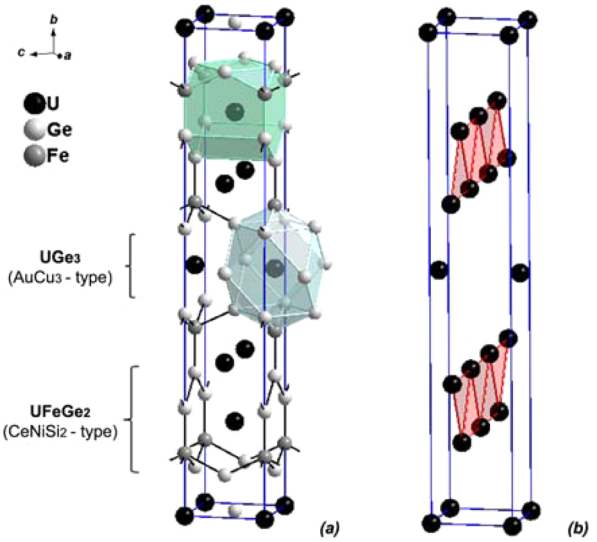

Figure 4. (a) Unit cell of $U_3Fe_2Ge_7$ and coordination polyhedra for the U1 (cyan) and U2 (green) atoms. The structure can be seen as a stacking of layers of $UFeGe_2$ and UGe_3 along the b axis. (b) Uranium sublattice showing the zigzag coordination of the U2 atoms.

$UFeGe_2$ intercalated by a fragment of UGe_3, as already described for other similar compounds (see, for example, ref 14).

In this structure there are two crystallographically nonequivalent sites for uranium atoms, 2*a* (U1) and 4*j* (U2). The coordination polyhedra for both of them are presented in Figure 4a. U1 is surrounded by 2 Fe and 12 Ge atoms forming a bicapped distorted cuboctahedron, whereas U2 is located in the center of a distorted hexagonal prism defined by 4 Fe and 10 Ge atoms. According to Table 3, all the distances between U and nearest neighbor atoms are above the sum of the metallic radii (r_U = 1.53 Å, r_{Fe} = 1.26 Å, and r_{Ge} = 1.39 Å[29]). Moreover, as can be seen in Figure 4a and b, U1 and U2 atoms have no other uranium atoms as nearest neighbors. The shortest distance is found between U2 atoms, as d_{U2-U2} = 3.9 Å in the *bc* plane, which is only slightly shorter than the U1−U1 bond length that coincides with the *a* lattice parameter. The second nearest d_{U2-U2} is equal to the lattice constant *c*. Therefore, the direct 5f−5f overlap is very weak, if any. The U−Ge hybridization is also expected to be weak in the UGe_3 building block of the crystal structure of $U_3Fe_2Ge_7$, as the distances between these atoms, 3 Å, are longer than the sum of their atomic radii. The exception is the bond length U1−Ge1 (2.94 Å), which is comparable with the sum of the atomic radii and of the order of the corresponding distances in the cubic UGe_3 compound (2.97 Å). Nevertheless, strong hybridization can be expected between the Fe-3d and Ge-4p states, as the distances between these atoms (∼2.3 Å) are found to be shorter than the sum of their atomic radii. Distances of the same order of magnitude are found between Co−Ge, Fe−Si, and Ru−Si in the ternary compounds $U_3Co_2Ge_7$, $U_3Fe_2Si_7$, and $U_3Ru_2Si_7$, respectively.[14,15,19,21] In the case of Ge, only the distances Ge2−Ge2 are below the double atomic radius of Ge. A similar situation is found in the ternary counterparts both with Ge and Si.

3.2. Magnetism. Figure 5 shows the temperature dependences of the magnetization, *M*, measured along the principal

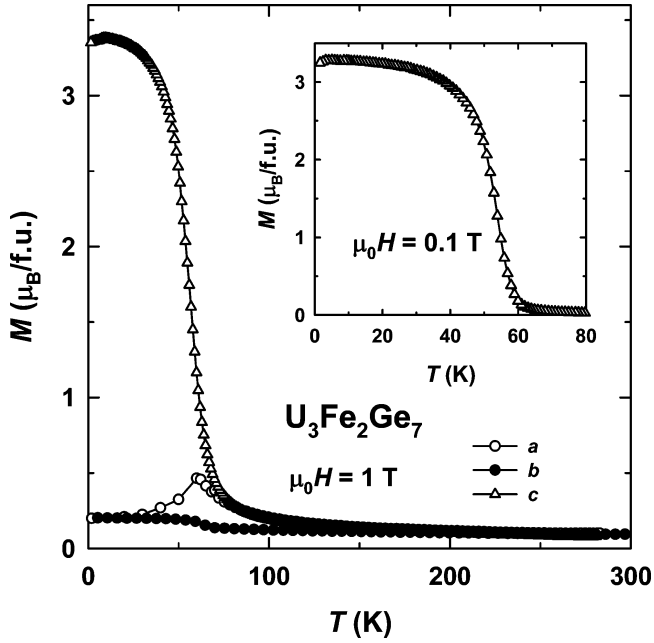

Figure 5. Temperature dependence of the magnetization along the *a*, *b*, and *c* axes of a $U_3Fe_2Ge_7$ single crystal in a field of 1 T. The inset shows the magnetization along the *c* axis in a field of 0.1 T.

crystallographic directions of $U_3Fe_2Ge_7$ in a magnetic field of 1 T. In this representation the increase of *M* observed along the *c* axis below 100 K, related to ferromagnetic ordering, dominates. The compound has a strong magnetic anisotropy with the highest magnetization values along the *c* axis. The magnetic ordering temperature, close to 60 K, can be distinguished from the $M(T)$ dependence along the *c* axis measured in a lower field of 0.1 T (inset in Figure 5).

The magnetic anisotropy of $U_3Fe_2Ge_7$ is illustrated by the magnetization curves (Figure 6). Only field descending branches are shown; the magnetic hysteresis will be discussed below. The compound exhibits a strong uniaxial magnetic anisotropy. The easy magnetization direction (EMD) is indeed along the *c* axis, where the spontaneous magnetic moment M_s = 3.3 μ_B/f.u. is reached at 2 K. In high fields the magnetization continues to grow approximately linearly as a function of field, probably due to an additional splitting of the spin-up and spin-down sub-bands. There are no spontaneous moment projections onto the *a* and *b* axes. Therefore, they both represent hard magnetization directions. Nevertheless, a

DOI: 10.1021/acs.inorgchem.5b01736
Inorg. Chem. 2015, 54, 9646−9655

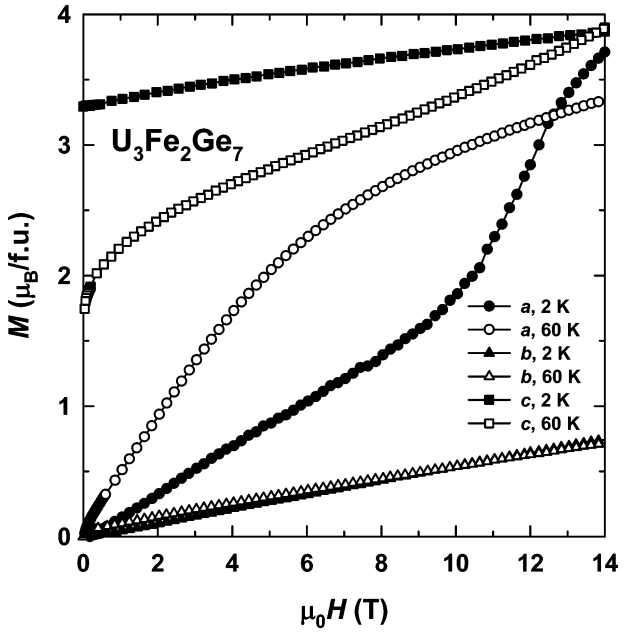

Figure 6. Magnetization curves along the *a*, *b*, and *c* axes of a $U_3Fe_2Ge_7$ single crystal at 2 and 60 K.

pronounced anisotropy is also observed within the *ab* plane, as the susceptibility, d*M*/d*H*, is much smaller along the *b* axis, the hardest magnetization direction, than along the *a* axis. A field-induced transition occurs along the *a* axis around 11 T, where the magnetization starts to increase faster. With increasing temperature the spontaneous magnetic moment decreases as follows from the *M*(*H*) dependence along the *c* axis at 60 K (Figure 6). At this temperature the field-induced transition along the *a* axis is no longer observed. The magnetization along the hardest *b* axis changes very little with temperature.

The U sublattice in the crystal structure of $U_3Fe_2Ge_7$ is coordinated in zigzag chains formed by the U2 atoms (Figure 4b). The chains are confined in the *ab* planes and propagate along the *a* direction. The U−U distance within the chains is 3.92 Å. The second and third shortest U−U distances coincide with the *c* (4.156 Å) and *a* (4.167 Å) lattice parameters, respectively. Since in uranium intermetallic compounds the uranium magnetic moments tend to be perpendicular to the shortest U−U bonds,[31,32] the EMD is the *c* axis, whereas the *a* and *b* axes are hard magnetization directions. Interestingly, in isostructural $U_3Co_2Ge_7$ the magnetic moments were found to be oriented along the *b* axis.[15−17] One can also compare the situation with UGe_2 crystallizing in the same space group (*Cmmm*, $ZrGa_2$-type), where uranium zigzag chains with the shortest U−U distances propagate along the *a* axis, as well.[30] However, in striking contrast to the presently studied compound, the magnetic moments are oriented along the *a* axis in the binary germanide.

Quite typical for uranium intermetallic compounds, $U_3Fe_2Ge_7$ displays an extremely strong magnetic anisotropy that reflects the complex bonding and hybridization in the system. As usual in such cases, the anisotropy field is so high that it cannot be easily estimated. At 2 K, a linear extrapolation of the *b*-axis magnetization to high fields indicates that it reaches the magnetization corresponding to M_s in the vicinity of 65 T. On the other hand, if one takes into consideration that along the easy-magnetization direction the magnetization increases in a magnetic field above M_s, the magnetization curves along the *b* and *c* axes intersect at a much higher field, around 250 T. This illustrates the fact that the simple picture of more or less well-defined magnetic moments that can be rotated by high fields out of the easy magnetization direction fails for U intermetallics.

In order to study the magnetic anisotropy in more detail, measurements of magnetization in pulsed high magnetic fields were performed (see Figure 7). One can see that while the field

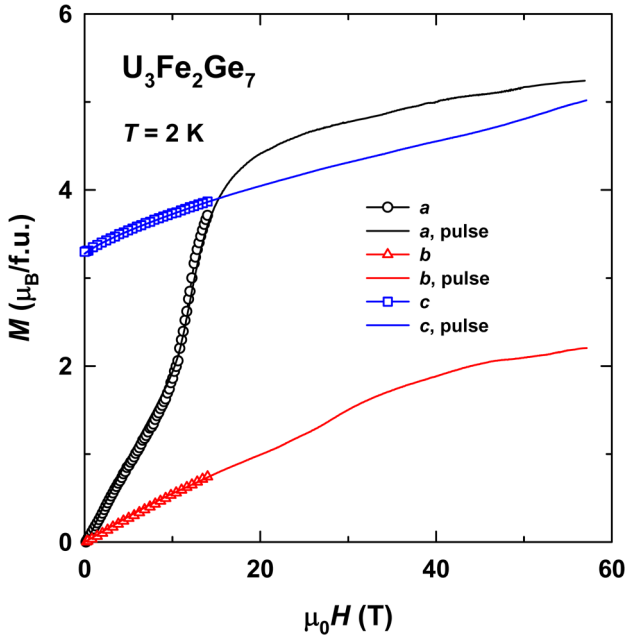

Figure 7. Magnetization curves along the *a*, *b*, and *c* axes of a $U_3Fe_2Ge_7$ single crystal in pulsed magnetic fields at 2 K. The symbols represent steady-field results.

applied along the *b* axis does not lead to any qualitative change, along *a* it induces a moment reorientation starting at about 12 T, and the high field magnetization even exceeds that along *c*. The differential magnetic susceptibility is approximately the same for all the directions above 20 T, suggesting that the same process, the splitting of the sub-bands by field, may be responsible for its value irrespective of field direction.

An attempt was made to approximate the temperature dependences of the inverse magnetic susceptibility, $1/\chi(T)$, calculated from the $M(T)$ curves in the paramagnetic range (Figure 5), by the modified Curie−Weiss law:

$$\chi = \chi_0 + C/(T - \theta_p) \quad (1)$$

where *C* is the Curie constant proportional to the effective magnetic moment, μ_{eff}; θ_p is the paramagnetic Curie temperature; and χ_0 is the temperature-independent term. Along the EMD the following values were obtained: $\mu^c_{eff} = 5.1\ \mu_B$/f.u. and $\theta^c_p = 54$ K. χ_0 was found to be the same, $\sim 4 \times 10^{-7}$ m^3 mol^{-1}, for all the directions. Along the *b* axis there is a very weak temperature dependence of the magnetic susceptibility. It can be formally described assuming a much higher effective magnetic moment, $\mu^b_{eff} = 9.1\ \mu_B$/f.u., and a large negative Weiss temperature, $\theta^b_p \approx -400$ K. Such a high effective moment is, however, unphysical. Rather, a weak Pauli paramagnetic response is a more likely explanation for the *b* direction. Many analogous cases can be found in other uranium-based strongly anisotropic intermetallic com-

DOI: 10.1021/acs.inorgchem.5b01736
Inorg. Chem. 2015, 54, 9646−9655

pounds.[31,32] By contrast, more reasonable values were found for the *a* axis according to eq 1: μ^a_{eff} = 6.3 μ_B/f.u. and θ^a_p = 28 K.

The field-induced transition along the hard *a* axis of $U_3Fe_2Ge_7$ at 2 K (Figures 6 and 7) is reminiscent of a first-order magnetization process (FOMP), e.g., a rotation of the magnetization vector due to the existence of two inequivalent minima of the free energy as a function of magnetic field.[33] This is a type-I FOMP since immediately above the transition the magnetization reaches the easy-axis value and even slightly exceeds it. The temperature evolution of the FOMP is shown in Figure 8. No hysteresis was detected at the transition. With

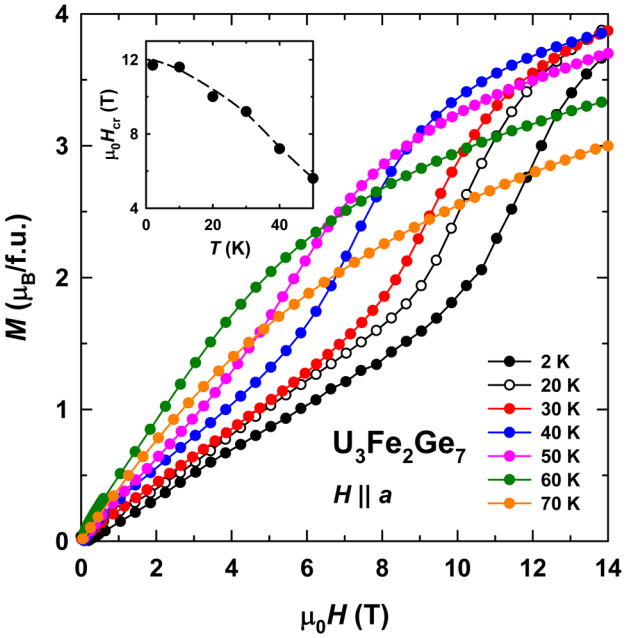

Figure 8. Temperature evolution of the magnetization curve along the *a* axis of a $U_3Fe_2Ge_7$ single crystal between 2 and 70 K. The inset shows the temperature dependence of the FOMP critical field.

increasing temperature the critical field of the transition, H_{cr}, decreases gradually. The H_{cr} values were determined from the d*M*/d*H* derivative. The FOMP is still observed at 50 K, but above this temperature it is no longer seen. The temperature dependence of the FOMP critical field is shown in the inset in Figure 8.

We can benefit from the FOMP-like transition since it provides a tool for the description of the magnetic anisotropy despite its enormous energetic strength, which makes for $U_3Fe_2Ge_7$ its direct measurement impossible. A FOMP can be described using the following relation:

$$HM_s = 2K_1(M/M_s) + 4K_2(M/M_s)^3 + 6K_3(M/M_s)^5 \quad (2)$$

where K_1, K_2, and K_3 are the second-, fourth-, and sixth-order anisotropy constants, respectively.[33] Since $U_3Fe_2Ge_7$ displays a type-I FOMP, K_3 should be zero. Using the sum of the two terms on the right side of eq 2, we succeeded in fitting the magnetization curves along the *a* axis in the temperature range between 2 and 60 K. A typical fit is shown in Figure 9 for 2 K. The anisotropy constants obtained from the fit are presented in the inset in Figure 9. Here, the constants are denoted K_1* and K_2* since they were determined for the *a* axis, whereas the corresponding values along the hardest (*b*) axis should be higher. At 2 K the constants are K_1* = 1.47 MJ/m^3 and K_2* = −0.34 MJ/m^3. Both K_1* and K_2* decrease gradually with temperature and approach zero in the vicinity of the magnetic ordering temperature. Along the hardest *b* axis we obtained K_1 ≈ 4.4 MJ/m^3 and K_2 > 0 at 2 K by the extrapolation of the *M*(*H*) curve beyond fields above 60 T and its intersection with the value of the spontaneous magnetic moment.

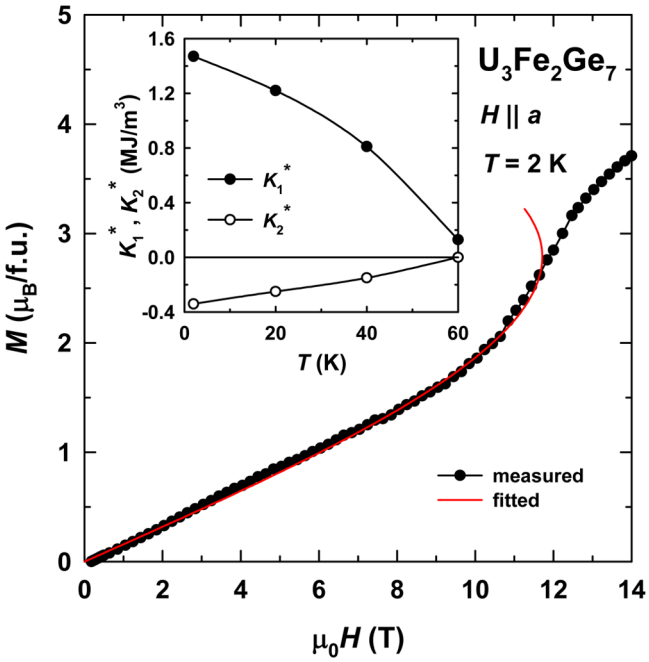

Figure 9. Magnetization curve along the *a* axis of a $U_3Fe_2Ge_7$ single crystal at 2 K. The red line represents the fit according to eq 2. The inset shows the temperature dependence of the anisotropy constants.

The temperature evolution of *M*(*H*) for the *c* axis of $U_3Fe_2Ge_7$ between 2 and 70 K is presented in Figure 10. The curves exhibit approximately the same high-field susceptibility at temperatures up to 50 K. At 60 K, the high-field susceptibility increases noticeably. At 70 K, the spontaneous magnetization is zero since the compound is already in the paramagnetic state. The $M_s(T)$ dependence (determined from Arrott plots) shown in the inset of Figure 10 is typical ferromagnetic. The spontaneous magnetic moment falls to zero at the Curie temperature, T_C = 62 K.

Hysteresis loops along the easy-magnetization direction of $U_3Fe_2Ge_7$ between 2 and 30 K are presented in Figure 11. $U_3Fe_2Ge_7$ displays a large magnetic hysteresis. The loop at 2 K displays a shape close to rectangular, but at higher temperatures the vertical loop branches for both field directions have a slightly different slope. The coercive field, μ_0H_c, reaches 2.3 T at 2 K and rapidly decreases with temperature. The inspection of the virgin curve at 2 K reveals that the pinning of narrow domain walls is very important. The abrupt increase of the magnetization around 1.7 T occurs when the applied magnetic field overcomes the potential barrier for domain walls pinned to defects. It should be pointed out that the coercive field exceeds the value of 1.7 T after a complete hysteresis cycle. This observation along with the stepwise remagnetization at H_c in positive and negative fields indicates that the dominant mechanism of the magnetic hysteresis is a reverse domain nucleation lag.

The observation of the strong magnetic anisotropy and hysteresis and of the FOMP transition suggests that the magnetism of $U_3Fe_2Ge_7$ is dominated by the uranium

DOI: 10.1021/acs.inorgchem.5b01736
Inorg. Chem. 2015, 54, 9646−9655

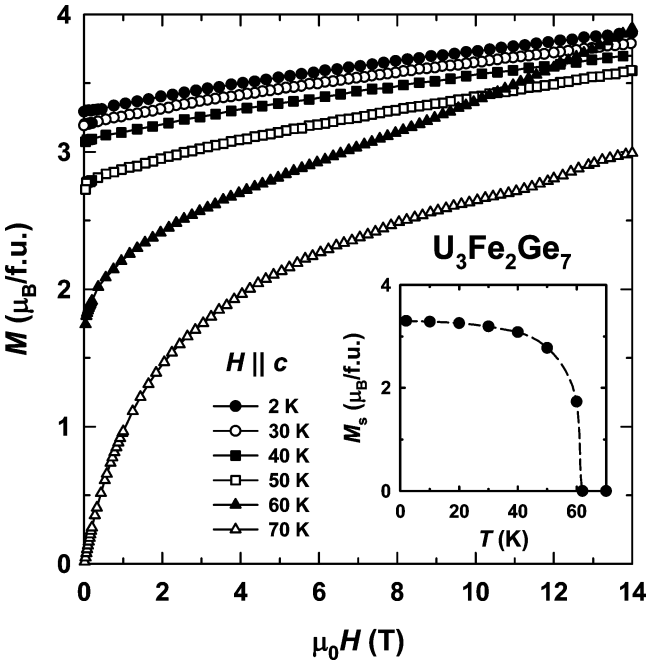

Figure 10. Temperature evolution of the magnetization curve along the *c* axis of a $U_3Fe_2Ge_7$ single crystal between 2 and 70 K. The inset shows the temperature dependence of the spontaneous magnetic moment.

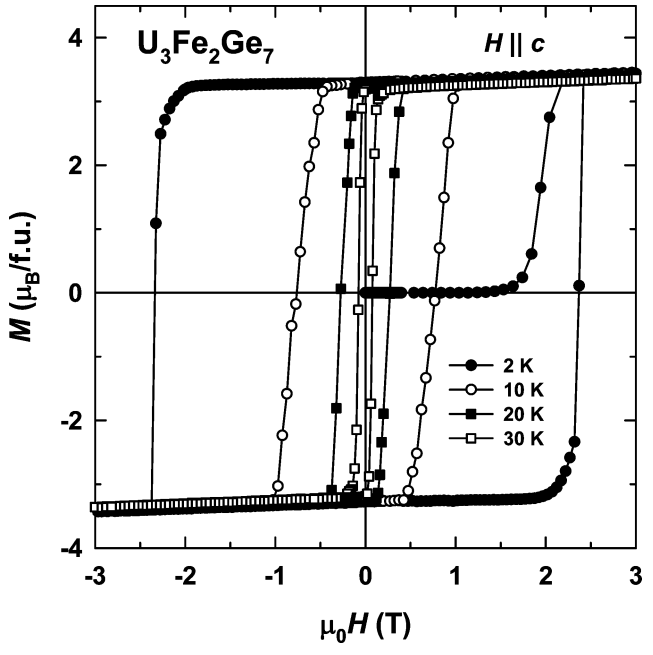

Figure 11. Hysteresis loops along the *c* axis of a $U_3Fe_2Ge_7$ single crystal between 2 and 30 K.

sublattice. Nevertheless, these data do not exclude the existence of ordered magnetic moments on the Fe atoms. In order to determine whether or not the iron sublattice is magnetically ordered in $U_3Fe_2Ge_7$, a ^{57}Fe Mössbauer spectroscopy study was undertaken.

3.3. Mössbauer Spectroscopy. The Mössbauer spectra taken above T_C = 62 K show a doublet (Figure 12). The estimated parameters are summarized in Table 4. This result is consistent with the Fe atoms located at a single crystallographic site with point symmetry lower than cubic, in agreement with

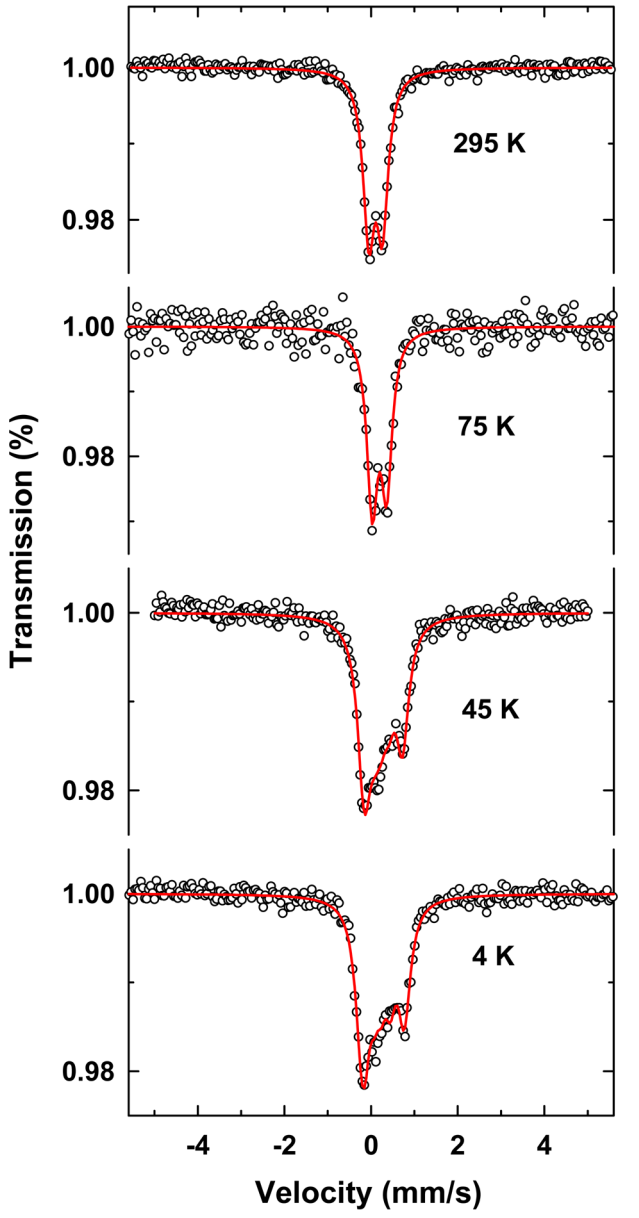

Figure 12. ^{57}Fe Mössbauer spectra of $U_3Fe_2Ge_7$ taken between 4 and 295 K.

Table 4. Estimated Parameters from the Mössbauer Spectra of $U_3Fe_2Ge_7$ Taken at Different Temperatures[a]

T (K)	IS (mm/s)	QS (mm/s)	2ε (mm/s)	B_{hf} (T)
295	0.21	0.32		
75	0.32	0.33		
45	0.32		0.12	2.8
4	0.33		0.12	3.1

[a]IS (mm/s) is the isomer shift relative to metallic α-Fe at 295 K; QS (mm/s) is the quadrupole splitting; $(2\varepsilon) = (e^2V_{ZZ}Q/4)(3\cos^2\theta - 1)$ (mm/s) is the quadrupole shift for the magnetic sextet; B_{hf} (tesla) is the magnetic hyperfine field. Estimated errors are ≤0.02 mm/s for IS, QS, and 2ε and ≤0.1 T for B_{hf}.

the structural data. At 45 K, below T_C, the spectrum envelope becomes significantly broader and can no longer be fitted by a doublet. The spectrum at 4 K is very similar. The 45 and 4 K spectra may be described as a magnetic sextet with small

DOI: 10.1021/acs.inorgchem.5b01736
Inorg. Chem. 2015, 54, 9646−9655

magnetic hyperfine field, B_{hf} = 2.8 and 3.1 T, respectively, similar to that observed in UFe_2.[34]

The nonzero B_{hf} value observed for the present compound below T_C (at 45 K) and the small increase of B_{hf} with decreasing temperature down to 4 K show that the Fe sublattice establishes long-range magnetic correlations below T_C. This behavior is different from several other U−Fe−Ge ternary ferromagnets, such as U_2Fe_3Ge,[8,9] $U_3Fe_4Ge_4$,[11,12] and $U_{34}Fe_{4-x}Ge_{33}$,[13] whose Mössbauer spectra below the corresponding magnetic ordering temperatures show no evidence of ordered Fe moments. This may be explained by a strong hybridization of the 3d(Fe) electrons with the 5f(U) electrons in U_2Fe_3Ge, $U_3Fe_4Ge_4$, and $U_{34}Fe_{4-x}Ge_{33}$, where the shortest Fe−U interatomic distances, d_{Fe-U}, are less than 3 Å. In the present $U_3Fe_2Ge_7$ compound the d_{Fe-U} value is higher, 3.202 Å (Table 3), only slightly lower than for UFe_6Ge_6 (3.27 Å), where the Fe sublattice is magnetically ordered below T_C = 322 K and shows a B_{hf} saturation value of 12.9 T,[35] significantly higher than in $U_3Fe_2Ge_7$. The high T_C of UFe_6Ge_6 when compared to $U_3Fe_2Ge_7$ may be related to the fact that in the former compound each Fe atom has four Fe nearest neighbors, while in $U_3Fe_2Ge_7$ the Fe atoms are isolated from each other.

Considering the hyperfine coupling constant of ∼15 T/μ_B, within the range common for these intermetallics,[7,8,13,35] the B_{hf} estimated at 4 K by the Mössbauer effect (Table 4) would be consistent with an iron magnetic moment $\mu_{Fe} \approx 0.2\ \mu_B$. For comparison, a lower magnetic moment, <0.1 μ_B, was inferred from *ab initio* calculations for the Co magnetic moment in $U_3Co_2Ge_7$.[16]

Using the results of the Mössbauer study we may conclude that if $U_3Fe_2Ge_7$ is a collinear ferromagnet, the magnetic moment of the uranium sublattice is around 2.9 μ_B/f.u. at 2 K. On average it corresponds to 0.97 μ_B per U atom. This value is considerably lower than the free-ion value, 3.2 and 3.3 μ_B, for the $5f^2$ and $5f^3$ configurations of uranium, respectively. This indicates that $U_3Fe_2Ge_7$ is an itinerant ferromagnet. Nevertheless, its moment is larger than in other ternary U−Fe−Ge intermetallics such as U_2Fe_3Ge (0.5 μ_B) and $U_3Fe_4Ge_4$ (0.4 μ_B).[9,11,12]

These results reinforce that due to the relatively large distances between U atoms, the 5f electrons are the main cause for the magnetism of $U_3Fe_2Ge_7$, since the establishment of robust magnetic order in the Fe sublattice is prevented by the extended Fe 3d−Ge 4p hybridization.

3.4. Specific Heat and Electrical Resistivity. The phase transition into the paramagnetic state of $U_3Fe_2Ge_7$ is reflected in the temperature dependencies of the specific heat, C_p (upper panel in Figure 13), and of the electrical resistivity, ρ (lower panel in Figure 13). $C_p(T)$ displays an anomaly that corresponds to a transition at 61 K, whereas $\rho(T)$ exhibits a steep downturn at the same temperature. The temperature derivative of the electrical resistivity, $d\rho/dT(T)$, has a sharp maximum at 60 K (lower panel in Figure 13).

The specific heat can be described by the expression

$$C_p = C_{el} + C_{ph} + C_{magn} \tag{3}$$

which represents the electronic, $C_{el} = \gamma T$, phonon, $C_{ph} = \beta T^3$, and magnetic, C_{magn}, contributions. From the extrapolation of the low-temperature part of the $C_p/T(T^2)$ function (upper inset in Figure 13) the Sommerfeld coefficient and the Debye temperature were found to be γ = 142 mJ mol^{-1} K^{-1} and Θ_D = 237 K, respectively. Alternatively, the Debye temperature was

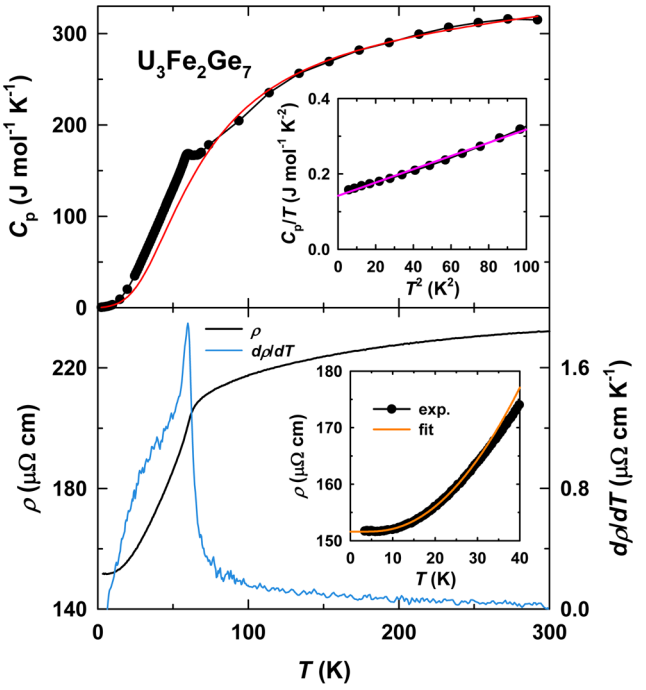

Figure 13. Temperature dependence of the specific heat (upper panel) and electrical resistivity (lower panel) of a $U_3Fe_2Ge_7$ single crystal. The upper inset shows the $C_p/T(T^2)$ function and the lower inset the $\rho(T)$ function and its fit according to eq 5 at low temperatures.

approximated by fitting $C_p(T)$ above the phase transition at T_C using the expression

$$C_{ph}(T) = \gamma T + 9NR(T/\Theta_D)^3 \int_0^{(\Theta_D/T)} [(x^4 e^x)/(e^x - 1)^2]\, dx \tag{4}$$

where the second term is the Debye integral with N being the number of atoms per formula unit (N = 12) and R the gas constant. The fit shown by the red line in the upper panel of Figure 13 yields Θ_D = 270 K. It should be noted that even such a simple model provides good agreement between the experimental and calculated curves above 100 K. The magnetic entropy can be roughly estimated to be S = 28 J mol^{-1} K^{-1}. This value exceeds $3R \ln(2)$ = 17.3 J mol^{-1} K^{-1} expected for a localized system with high uniaxial anisotropy, where only the U atoms carry a magnetic moment. It may hint at a nonzero contribution of moments of the Fe sublattice, in agreement with the results of the Mössbauer study.

Since $U_3Fe_2Ge_7$ is a strongly anisotropic ferromagnet with one hard magnetization axis and less pronounced anisotropy energy between the easy and intermediate axis, we can expect excitation of magnons over a gap corresponding to the anisotropy within the *ac* plane. Between 2 and 25 K, $C_p(T)$ can be fitted by the expression

$$C_p(T) = \gamma T + \beta T^2 + \delta T^{3/2} \exp(-\Delta_1/T) \tag{5}$$

where the last term takes into account the contribution of magnons with an energy gap Δ_1 = 24 K (δ = 0.11 J mol^{-1} K$^{-5/2}$). The obtained Δ_1 value is in good agreement with the magnetic anisotropy energy between the two easiest axes of $U_3Fe_2Ge_7$, *a* and *c*: $\theta^c_p - \theta^a_p$ = 54 − 28 = 26 K.

The electrical resistivity of $U_3Fe_2Ge_7$ displays metallic values (lower panel in Figure 13) consistent with the dominance of

DOI: 10.1021/acs.inorgchem.5b01736
Inorg. Chem. 2015, 54, 9646−9655

metallic bonds in this compound. Between 2 and 20 K, $\rho(T)$ can be approximated by the following equation:

$$\rho(T) = \rho_0 + aT^2 + bT(1 + 2T/\Delta_2)\exp(-\Delta_2/T) \quad (6)$$

where the first term is the residual resistivity, the second term describes the electron−electron scattering, and the third term takes into account the scattering of the conduction electrons on magnons (Δ_2 is the gap of magnons with the lowest energy).[36] The best fit of the experimental data is shown by the orange line in the lower inset in Figure 13. The following parameters were obtained for this curve: ρ_0 = 152 $\mu\Omega$ cm, $a = 7.3 \times 10^{-7}$ $\mu\Omega$ cm K^{-2}, b = 0.2418 $\mu\Omega$ cm K^{-1}, and Δ_2 = 22 K. The residual resistivity is high, probably due to a certain atomic disorder. Such a situation makes the analysis of $\rho(T)$ in terms of individual contributions difficult; their additivity cannot be assumed as given. Nevertheless, the low-temperature part can be described by a dominating term attributed to the electron−magnon scattering, while the electron−phonon contribution can be neglected in this temperature range. The Δ_2 value is in good agreement with that deduced from the specific heat, 24 K, and from the anisotropy energy (per one ion), 26 K, between the a and c axes of $U_3Fe_2Ge_7$.

4. CONCLUSIONS

A $U_3Fe_2Ge_7$ single crystal (orthorhombic crystal structure of $La_3Co_2Sn_7$ type) has been successfully synthesized by the flux method. $U_3Fe_2Ge_7$ orders ferromagnetically at T_C = 62 K. The U atoms are arranged in zigzag chains in the ab plane, which forces the U magnetic moments along the perpendicular c axis due to the two-ion hybridization-induced anisotropy. The easy magnetization direction distinguishes $U_3Fe_2Ge_7$ from other U-based isostructural compounds where the magnetic moments are oriented along the b axis. In $U_3Fe_2Ge_7$, both the U and Fe sublattices are ordered, yielding a spontaneous magnetic moment of 3.3 μ_B per formula unit at 2 K. The compound exhibits a first-order magnetization process that makes it possible to quantify the huge magnetic anisotropy with the anisotropy field above 60 T. The gap in the magnon spectrum that follows from the specific heat and electrical resistivity complies with the strong magnetic anisotropy.

■ ASSOCIATED CONTENT

Supporting Information

The Supporting Information is available free of charge on the ACS Publications website at DOI: 10.1021/acs.inorgchem.5b01736.

Crystallographic information file (CIF)

■ AUTHOR INFORMATION

Corresponding Authors

*E-mail: henriques@fzu.cz (M. S. Henriques).
*E-mail: d.gorbunov@hzdr.de (D. I. Gorbunov).

Author Contributions

The manuscript was written through contributions of all authors.

Notes

The authors declare no competing financial interest.

■ ACKNOWLEDGMENTS

D.I.G. and A.V.A. performed the measurements of the electronic properties in the MLTL (http://mltl.eu/), which is supported within the program of Czech Research Infrastructures, Project No. LM2011025; they also received funding from the Czech Academy of Sciences (project M10010203). M.S.H. is grateful for the funding of the Czech Science Foundation (project 14-03276S) and the Portuguese Foundation for Science and Technology through the grant SFRH/BD/66161/2009. We acknowledge the support of the High Magnetic Field Laboratory Dresden (HLD) at HZDR, member of the European Magnetic Field Laboratory (EMFL).

■ REFERENCES

(1) Andreyev, A. V.; Bartashevich, M. I. *Phys. Met. Metallogr.* **1986**, *62* (N2), 50−53.
(2) Popov, Y. F.; Levitin, R. Z.; Deryagin, A. V.; Zeleny, M.; Andreev, A. V. *Sov. Phys. JETP* **1980**, *51*, 1223.
(3) Hamaguchi, Y.; Kunitomi, N.; Komura, S.; Sakamato, M. *J. Phys. Soc. Jpn.* **1962**, *17*, 398−398.
(4) Yessik, M. *J. Appl. Phys.* **1969**, *40*, 1133−1135.
(5) Henriques, M. S.; Berthebaud, D.; Lignie, A.; El Sayah, Z.; Moussa, C.; Tougait, O.; Havela, L.; Gonçalves, A. P. *J. Alloys Compd.* **2015**, *639*, 224−234.
(6) Henriques, M. S.; Berthebaud, D.; Pereira, L. C. J.; Lopes, E. B.; Branco, M. B. C.; Noël, H.; Tougait, O.; Šantavá, E.; Havela, L.; Carvalho, P. A.; Gonçalves, A. P. *Intermetallics* **2011**, *19*, 841−847.
(7) Dhar, S. K.; Shah, K. V.; Bonville, P.; Manfrinetti, P.; Wrubl, F. *Solid State Commun.* **2008**, *147*, 217−220.
(8) Henriques, M. S.; Tougait, O.; Noël, H.; Pereira, L. C. J.; Waerenborgh, J. C.; Gonçalves, A. P. *Solid State Commun.* **2008**, *148*, 159−162.
(9) Henriques, M. S.; Gorbunov, D. I.; Waerenborgh, J. C.; Havela, L.; Shick, A. B.; Diviš, M.; Andreev, A. V.; Gonçalves, A. P. *J. Phys.: Condens. Matter* **2013**, *25*, 066010-1−066010-9.
(10) Henriques, M. S.; Gorbunov, D. I.; Andreev, A. V.; Arnold, Z.; Surblé, S.; Heathman, S.; Griveau, J.-C.; Lopes, E. B.; Prchal, J.; Havela, L.; Gonçalves, A. P. *Phys. Rev. B: Condens. Matter Mater. Phys.* **2014**, *89*, 054407-1−054407-9.
(11) Berthebaud, D.; Tougait, O.; Potel, M.; Lopes, E. B.; Waerenborgh, J. C.; Gonçalves, A. P.; Noël, H. *J. Alloys Compd.* **2013**, *554*, 408−413.
(12) Henriques, M. S.; Gorbunov, D. I.; Waerenborgh, J. C.; Havela, L.; Andreev, A. V.; Skourski, Y.; Gonçalves, A. P. *J. Alloys Compd.* **2013**, *555*, 304−310.
(13) Henriques, M. S.; Berthebaud, D.; Waerenborgh, J. C.; Lopes, E. B.; Pasturel, M.; Tougait, O.; Gonçalves, A. P. *J. Alloys Compd.* **2014**, *606*, 154−163.
(14) Dörrscheidt, W.; Schäfer, H. *J. Less-Common Met.* **1980**, *70*, P1−P10.
(15) Bobev, S.; Bauer, E. D.; Ronning, F.; Thompson, J. D.; Sarrao, J. L. *J. Solid State Chem.* **2007**, *180*, 2830−2837.
(16) Uhlířová, K.; Diviš, M.; Pospíšil, J.; Sechovský, V. *J. Phys. Conf. Series* **2010**, *9*, 012048-1−012048-6.
(17) Uhlířová, K.; Diviš, M.; Pospíšil, J.; Daniš, S.; Sechovský, V. *J. Phys. Soc. Jpn.* **2012**, *81*, 094703−1−094703−10.
(18) Akselrud, L. G.; Yarmolyuk, Y. P.; Rozhdestvenskaya, I. V.; Gladyshevsky, E. I. *Kristallografiya* **1981**, *26*, 186−188.
(19) Berthebaud, D.; Lopes, E. B.; Tougait, O.; Gonçalves, A. P.; Potel, M.; Noël, H. *J. Alloys Compd.* **2007**, *442*, 348−350.
(20) Berthebaud, D.; Tougait, O.; Gonçalves, A. P.; Noël, H. *Intermetallics* **2008**, *16*, 373−377.
(21) Pasturel, M.; Pikul, A. P.; Potel, M.; Roisnel, T.; Tougait, O.; Noël, H.; Kaczorowski, D. *J. Solid State Chem.* **2010**, *183*, 1884−1890.
(22) Pöttgen, R.; Chevalier, B.; Gravereau, P.; Darriet, B.; Jeitschko, W.; Etourneau, J. *J. Solid State Chem.* **1995**, *115*, 247−254.
(23) *CryAlis PRO*, Version 1.171.37.31; Agilent Technologies, 2014.
(24) *X-Shape 1.06*, Crystal Optimisation for Numerical Absorption Correction (C); Stoe & Cie GmbH: Darmstadt, Germany, 1999.
(25) Palatinus, L.; Chapuis, G. *J. Appl. Crystallogr.* **2007**, *40*, 786−790.

DOI: 10.1021/acs.inorgchem.5b01736
Inorg. Chem. 2015, 54, 9646−9655

(26) Petříček, V.; Dušek, M.; Palatinus, L. *Z. Kristallogr. - Cryst. Mater.* **2014**, *229*, 345−352.
(27) Hahn, Th. In *International Tables for Crystallography*, Vol. A; Hahn, Th., Ed.; Springer: The Netherlands, 2002.
(28) Waerenborgh, J. C.; Gonçalves, A. P.; Bonfait, G.; Godinho, M.; Almeida, M. *Phys. Rev. B: Condens. Matter Mater. Phys.* **1999**, *60*, 4074−4081.
(29) Vainshtein, B. K.; Fridkin, V. M.; Indenbom, V. L. *Structure of Crystals, Modern Crystallography*, Vol. *2*; Springer-Verlag: Berlin, 2000.
(30) Aoki, D.; Flouquet, J. *J. Phys. Soc. Jpn.* **2012**, *81*, 011003−1−011003−11.
(31) Sechovský, V.; Havela, L. In *Handbook of Magnetic Materials*, Vol. *4*; Wohlfarth, E. P.; Buschow, K. H. J., Eds.; Elsevier: Amsterdam, 1988.
(32) Sechovský, V.; Havela, L. In *Handbook of Magnetic Materials*, Vol. *11*; Buschow, K. H. J., Ed.; Elsevier: Amsterdam, 1998.
(33) Asti, G. In *Handbook of Magnetic Materials*, Vol. *5*; Buschow, K. H. J.; Wohlfarth, E. P., Eds.; Elsevier: Amsterdam, 1990.
(34) Gal, J.; Hadari, Z.; Bauminger, E. R.; Nowik, I.; Ofer, S.; Perkal, M. *Phys. Lett. A* **1970**, *31*, 511−512.
(35) Gonçalves, A. P.; Waerenborgh, J. C.; Bonfait, G.; Amaro, A.; Godinho, M. M.; Almeida, M.; Spirlet, J. C. *J. Alloys Compd.* **1994**, *204*, 59−64.
(36) Andersen, N. H.; Smith, H. *Phys. Rev. B: Condens. Matter Mater. Phys.* **1979**, *19*, 384−387.

DOI: 10.1021/acs.inorgchem.5b01736
Inorg. Chem. 2015, 54, 9646−9655